NASA TECHNICAL
MEMORANDUM

NASA TM X-3114

NASA TM X-3114

THEORETICAL SURFACE VELOCITY DISTRIBUTIONS ON ACOUSTIC SPLITTER GEOMETRIES FOR AN ENGINE INLET

by James A. Albers and Douglas C. Breunlin

Lewis Research Center
Cleveland, Ohio 44135

NATIONAL AERONAUTICS AND SPACE ADMINISTRATION • WASHINGTON, D. C. • OCTOBER 1974

THEORETICAL SURFACE VELOCITY DISTRIBUTIONS ON ACOUSTIC

SPLITTER GEOMETRIES FOR AN ENGINE INLET

by James A. Albers and Douglas C. Breunlin

Lewis Research Center

SUMMARY

This report presents the results of an analytical study of the potential-flow velocity distributions on several splitter geometries in an engine inlet and their variation with different splitter leading edge shapes and distances from the inlet highlight. The velocity distributions on the inner and outer surfaces of the splitters are presented for low-speed and cruise conditions. The results indicate that, at both cruise and low-speed conditions at zero incidence angle, the splitter with the 4-to-1 elliptical leading edge had lower peak velocities and velocity gradients than the splitter with the 2-to-1 elliptical leading edge. The velocity gradients on the inner and outer surfaces decreased as the distance from the inlet highlight to the splitter leading edge was increased. For a given distance, the peak velocity on the splitter inner surface increased with increasing inlet incidence angle. At an incidence angle of 50°, the velocity level and gradients on the inner surface of the splitter in the forward position were sufficiently severe to suggest local separation.

INTRODUCTION

A continuing problem in the development of airbreathing propulsion systems is the design of the engine inlet. This inlet must provide high-pressure recovery, low total-pressure distortion, and uniform flow to the engine throughout the entire flight envelope. Required aircraft noise levels also dictate, in most cases, the application of sound-absorbing material within the inlet. Some applications currently require sound-absorbing concentric splitter rings to meet noise goals during takeoff and landing. The integration of these concentric splitter rings into the inlet system presents a major challenge to the inlet designer. Thus, there is a definite need to establish aerodynamic guidelines for the location and shape of acoustic splitters.

This report presents the results of an analytical study of the velocity distributions on several splitter geometries in an engine inlet. The analysis uses an incompressible potential-flow solution corrected for compressibility (ref. 1). The inlet geometry including the splitter was axisymmetric.

The splitter geometric variables investigated were the shape and axial location of the splitter leading edge. The velocity distributions on the inner and outer surfaces of the splitter are presented for low-speed and cruise conditions. For low-speed conditions, the free-stream Mach number was 0.12 with incidence angles of 0° and 50°. For the incidence angle of 50°, the velocity distributions along the splitter are presented at several circumferential locations. For cruise conditions, the free-stream Mach number was 0.75 with an incidence angle of 0°.

SYMBOLS

A_f fan annular area

L splitter length

R radial distance from inlet axis

V velocity on surface of splitter

V_{ref} reference velocity, equal to 304.8 m/sec (1000 ft/sec)

V_∞ free-stream velocity

w_{cor} weight flow corrected for temperature and pressure

X distance from inlet highlight

X' distance from fan face

α incidence angle at inlet, direction of free-stream velocity relative to inlet axis

ψ circumferential angle around inlet

Subscripts:

h highlight

i inside of splitter

le leading edge

o outside of splitter

p peak

2

INLET AND SPLITTER GEOMETRY

An illustration of the inlet with the splitter geometries considered in this investigation is shown in figure 1. The inlet configuration is a conventional subsonic inlet with an NACA-series-1 external cowl shape and a 2-to-1 ellipse internal lip. The contraction ratio (highlight area to throat area) is 1.35, which provides a good angle-of-attack tolerance (ref. 2). The maximum cowl diffuser surface angle is 10°, and the diffuser effective cone angle is 4.4^O. The inlet centerbody has an NACA-series-1 contour, with the leading edge of the centerbody downstream of the cowl throat. The details of the cowl and centerbody coordinates are given in figures 2 and 3 of reference 3.

The splitters are located on the inlet cruise streamline which bisects the height of the annular flow passage at the fan face. Locating the splitters on the cruise streamline minimizes the pressure loss due to the splitters at cruise conditions. From the point of view of acoustic design calculations, equal passage heights (cowl to splitter and splitter to centerbody) are desired. The cruise streamline which bisects the flow passage at the fan face defines the mean line of the splitters and splits the flow so that 42 percent is in the inner passage and 58 percent is in the outer passage.

Table I summarizes the inlet splitter geometric variables considered in this investigation. The splitter leading and trailing edges are illustrated in figure 2. The detailed coordinates for the inlet splitters are given in tables II to IX. The splitters are designated as 1-2, 1-4, 2-4, and 3-4, where the first number refers to the splitter leading-edge location and the second refers to the shape of the leading edge (either a 2-to-1 or 4-to-1 ellipse). The inlet-highlight-to-splitter-leading-edge spacings X_{le} for the three splitters were 0.25, 0.50, and 0.75 of the highlight radius R_h. The fan-face-to-splitter-trailing-edge spacing was held constant at an X'/R_h of 0.1. The corresponding nondimensional lengths L/R_h were 1.05, 0.80, and 0.55, respectively. Two leading-edge geometries were selected for the longest splitter: a 2-to-1 elliptical leading edge (fig. 2(a)) and a 4-to-1 elliptical leading edge (fig. 2(b)). The 4-to-1 elliptical leading edge was chosen for the two shorter length splitters (figs. 2(c) and (d)).

The splitter walls were developed by adding 1.5 percent of the highlight radius to the mean line. This resulted in a splitter thickness of 3 percent of the highlight radius. The elliptical leading edges of the splitters were positioned at angles coincident with the local angles of flow at the coordinates of the splitter leading edge. Segments of superellipses were used to fair the leading-edge surfaces into the splitter main-body surface.

The splitter trailing edge (common to all four splitters) consisted of circular arcs with a mean-line angle defined by the tangent to the cruise streamline at the trailing edge (fig. 2(e)). The arcs used had local angles of less than 10° with respect to the mean line.

CALCULATION PROCEDURE

The Douglas Neumann program was used as the basis for calculating the incompressible potential-flow velocity distributions on the surfaces of the splitters. The method of solution (refs. 4 and 5) utilizes a distribution of sources on the inlet and splitter surfaces and solves for the source distribution that makes the normal component of velocity equal zero on the splitter and inlet surfaces. The potential-flow solution treats the splitter in the identical manner as the inlet surface. Three basic solutions for flow through the inlet with the splitter (fig. 1) were obtained. These solutions were (1) for axial flow with the inlet duct extension closed, (2) for axial flow with the duct open, and (3) for the crossflow ($\alpha \neq 0$) solution with the duct extension open. These three basic solutions were then combined to give a solution for any free-stream velocity, any mass flow rate through the inlet, and any inlet incidence angle. The incompressible potential-flow solution was corrected for compressibility by the use of the Lieblein-Stockman compressibility correction method of reference 6.

The preceding potential-flow method treats the inlet splitter as a nonlifting body (i.e., the Kutta condition is not satisfied at the splitter trailing edge). The achievement of a precise matching of the trailing-edge velocities at the trailing edge would require the addition of a ring vortex of appropriate strength, which was not incorporated in this analysis. Such a vortex would increase the magnitude of the inner-surface velocity and decrease the magnitude of the outer-surface velocity, thus increasing the velocity difference between the two surfaces. However, it was deemed that the relative trends shown by the present analysis would be unchanged by the requirement to match the trailing-edge velocities.

In order to minimize velocity differences between the inner and outer surfaces, the entire splitter mean line was alined along a flow streamline of the inlet without the splitter. The design streamline was taken as the 42 percent flow streamline from the inlet hub for the cruise condition.

DISCUSSION OF RESULTS

The surface velocity distributions on the splitters for cruise conditions at zero incidence angle are presented first because this is the design condition. This is followed by a discussion of the surface velocity distribution for low-speed conditions at zero incidence angle. Finally, the surface velocity distribution on the splitters at high incidence angle is discussed.

Cruise Condition

Surface velocity distributions on the inner and outer surfaces of the four splitter configurations at cruise conditions are shown in figure 3. For the case of the splitters located on a cruise streamline, relatively small velocity differences existed between the inner and outer surfaces. However, the peak velocity and velocity gradients were slightly higher on the splitter inner surface. The peak velocity difference on the inner and outer surfaces was less than 10 percent of peak velocity for all splitter geometries, indicating that the splitter was relatively well alined with the flow. The velocity differences between the inner and outer surfaces may be attributed to the thickness distribution of the splitter. The velocity difference may be reduced by reshaping the leading-edge geometry or by a slight positive incidence of the splitter leading edge from the mean line.

For the most forward leading-edge position, the splitter with the 4-to-1 elliptical leading edge (fig. 3(b)) had lower peak velocities and velocity gradients than the splitter with the 2-to-1 elliptical leading edge (fig. 3(a)). As the leading edge of the splitter was moved further into the inlet duct, the velocity level and gradients decreased slightly on the surface of the splitter (figs. 3(b) to (d)).

Low-Speed Condition

Zero incidence angle. - Surface velocity distributions on the inlet splitters are presented in figure 4 for low-speed conditions and at zero incidence angle. The peak velocity and velocity gradients were lower at low-speed conditions (fig. 4) than at cruise condition (fig. 3) since the takeoff weight flow was lower than the cruise weight flow (w_{cor}/A_f of 175 compared to 202 kg/(sec)(m^2)). As at cruise conditions, higher velocities were obtained on the inner surface of the splitter. The splitter with the 2-to-1 elliptical leading edge (fig. 4(a)) had higher velocities and velocity gradients on the inner and outer surfaces than the splitter with the 4-to-1 elliptical leading edge (fig. 4(b)). The velocity gradients on the inner and outer surfaces decreased as the splitter leading-edge distance from the inlet highlight was increased from 0.25 to 0.75 (figs. 4(b) to (d)). The velocity distributions were relatively constant on the inner and outer surfaces over most of the splitter surface.

50° Incidence angle. - Surface velocity distributions on the inlet splitters on the windward side of the inlet ($\psi = 0°$) are shown in figure 5 at 50° incidence angle. The highest velocity levels and gradients occurred on the inner surface of the splitter. The values at 50° incidence angle were substantially higher than those at zero incidence angle at both low speed and cruise speed. The large velocity gradients shown in figures 5(a) and (b) are indicative of possible local separation. These large gradients are a

5

result of the stagnation point on the splitter shifting further under the outside splitter surface ($\psi = 0^O$). The velocity distribution for the inlet splitter with the 2-to-1 elliptical leading edge (fig. 5(a)) was nearly the same as that for the 4-to-1 elliptical leading edge (fig. 5(b)). Thus, at 50° incidence angle the velocity distribution was insensitive to leading-edge geometry. However, the 2-to-1 ellipse is probably preferable from the point of view of available backing depth for acoustic treatment.

The peak velocity and velocity gradients were significantly reduced as the splitter leading edge was placed further into the inlet duct (figs. 5(c) and (d)). The effective flow incidence angle at the splitter leading edge decreased as the splitter leading edge was moved further aft in the inlet duct.

Surface velocity distributions on the splitter inner surface at various circumferential angles are presented in figure 6. A large variation in velocity distributions was obtained around the circumference of the inner splitter surface. For example, the peak velocity ratio decreased from 1.390 to 0.855 as the circumferential angle varied from 0° to 90° and further decreased to 0.645 at 180° (fig. 6(b)). The peak velocity ratio at $\psi = 90^O$ and 50° incidence angle is approximately the same as that at 0° incidence angle.

Peak velocity variation. - A summary plot for low-speed conditions is shown in figure 7. The peak velocity ratio is given as a function of a nondimensional distance from the inlet highlight X_{le}/R_h for $\psi = 0^O$. The velocity level on the surface for nacelle incidence angles of 50° and 30° decreased markedly as the distance of the splitter leading edge from the inlet highlight was increased from 0.25 to 0.50 and decreased further as the distance was increased to 0.75. Smaller variations in peak velocity were obtained at incidence angles of 10° and 0° as the distance of the splitter leading edge from the inlet highlight was increased from 0.25 to 0.75. For a given free-stream velocity, the local incidence angle at the splitter leading edge decreased as it was moved further into the inlet duct. For inlets required to operate at high incidence angles, it is therefore desirable to locate the splitter leading edge as far back in the inlet duct as acoustic requirements permit.

SUMMARY OF RESULTS

Theoretical velocity distributions on the inner and outer surfaces of several acoustic concentric splitters located in an inlet of an engine nacelle have been presented. The splitter variables investigated were the shape and axial location of the splitter leading edge. The splitters were located on the cruise streamline of the inlet which bisects the height of the annular passage at the fan face. The results were presented for both cruise and low-speed conditions. For cruise conditions the free-stream Mach number was 0.75 and the corrected weight flow per unit annular area was 202 kg/(sec)(m^2) with an incidence angle of 0°. For low-speed conditions the free-stream Mach number was

0. 12 and the corrected weight flow per unit annular area was 175 kg/(sec)(m^2) with incidence angles of 0° and 50°. The following results were observed:

1. At cruise conditions, relatively small differences existed in the velocity distribution on the inner and outer surfaces, indicating proper splitter alinement.

2. At both cruise and low-speed conditions at zero incidence angle, the splitter with the 4-to-1 elliptical leading edge had lower peak velocities and velocity gradients than the splitter with the 2-to-1 elliptical leading edge.

3. At 50° incidence angle, the velocity level and gradients were more severe on the inner surface of the splitter than they were at zero incidence angle. The large gradients obtained for some splitter locations were indicative of possible local separation. Also, large variations in velocity were obtained around the circumference of the splitter surface at high incidence angles. At 50° incidence angle, the velocity distributions were insensitive to leading-edge geometry.

4. The velocity gradients on the inner and outer surfaces decreased as the distance from the inlet highlight to the splitter leading edge was increased. For inlets required to operate at high incidence angles, it is desirable to locate the leading edge of the splitter as far back in the inlet duct as acoustic requirements permit.

Lewis Research Center,
National Aeronautics and Space Administration,
Cleveland, Ohio, July 18, 1974,
501-24.

REFERENCES

1. Albers, James A.; and Stockman, Norbert O.: Calculation Procedures for Potential and Viscous Flow Solutions for Engine Inlets. ASME Paper 74-GT-3, ASME, Mar. 1974.

2. Albers, James A.; and Miller, Brent A.: Effect of Subsonic Inlet Lip Geometry on Predicted Surface and Flow Mach Number Distributions. NASA TN D-7446, 1973.

3. Albers, James A.: Comparison of Predicted and Measured Low Speed Performance of Two 51-Centimeter-Diameter Inlets at Incidence Angle. NASA TM X-2937, 1973.

4. Stockman, Norbert O.; and Button, Susan L.: Computer Programs for Calculating Potential Flow in Propulsion System Inlets. NASA TM X-68278, 1973.

5. Hess, J. L.; and Smith, A. M. O.: Calculation of Potential Flow About Arbitrary Bodies. Progress in Aeronautical Sciences, vol. 8, D. Küchemann, ed., Pergamon Press, 1967, pp. 1-138.

6. Lieblein, S.; and Stockman, N. O.: Compressibility Correction for Internal Flow Solutions. J. Aircraft, vol. 9, no. 4, Apr. 1972, pp. 312-313.

TABLE I. - INLET SPLITTER GEOMETRIC VARIABLES

CONSIDERED IN THIS INVESTIGATION

[Splitter trailing-edge shape, circular arcs; splitter thickness, percent of highlight radius R_h, 3; location of splitter trailing edge, nondimensional distance from upstream of fan face, X'/R_h, 0.1.]

Splitter identification[a]	Nondimensional splitter length, L/R_h	Splitter leading-edge shape, type of ellipse	Location of splitter leading edge, nondimensional distance from inlet highlight, X_{le}/R_h
1-2	1.05	2-to-1	0.25
1-4	1.05	4-to-1	.25
2-4	.80	4-to-1	.50
3-4	.55	4-to-1	.75

[a]First number refers to splitter leading-edge location and second number refers to elliptical shape.

TABLE II. - LEADING EDGE COORDINATES - SPLITTER 1-2

Nondimensional distance from inlet highlight, X/R_h	Nondimensional distance from inlet axis		Nondimensional distance from inlet highlight, X/R_h	Nondimensional distance from inlet axis	
	For outside surface of splitter, R_o/R_h	For inside surface of splitter, R_i/R_h		For outside surface of splitter, R_o/R_h	For inside surface of splitter, R_i/R_h
0.2500	0.5741	0.5741	0.2650	0.5871	0.5611
.2505	.5768	.5714	.2700	.5882	.5600
.2510	.5779	.5703	.2750	.5889	.5593
.2520	.5795	.5687	.2800	.5891	.5591
.2530	.5806	.5676	.3100	.5891	.5591
.2540	.5816	.5666	.3155	.5892	.5592
.2550	.5824	.5658	.3193	.5893	.5593
.2560	.5831	.5651	.3251	.5895	.5595
.2570	.5837	.5645	.3290	.5897	.5597
.2580	.5843	.5639	.3349	.5899	.5599
.2590	.5848	.5634	.3408	.5902	.5602
.2600	.5853	.5629	.3447	.5904	.5604
.2625	.5863	.5619	.3500	.5907	.5607

8

TABLE III. - LEADING-EDGE COORDINATES - SPLITTER 1-4

Nondimensional distance from inlet highlight, X/R_h	Nondimensional distance from inlet axis		Nondimensional distance from inlet highlight, X/R_h	Nondimensional distance from inlet axis	
	For outside surface of splitter, R_o/R_h	For inside surface of splitter, R_i/R_h		For outside surface of splitter, R_o/R_h	For inside surface of splitter, R_i/R_h
0.2500	0.5741	0.5741	0.2800	0.5871	0.5611
.2505	.5760	.5722	.2850	.5877	.5605
.2510	.5768	.5714	.2900	.5882	.5600
.2520	.5779	.5703	.2950	.5886	.5596
.2530	.5788	.5694	.3000	.5889	.5593
.2540	.5795	.5687	.3050	.5890	.5591
.2550	.5801	.5681	.3100	.5891	.5591
.2560	.5806	.5676	.3155	.5892	.5592
.2570	.5811	.5671	.3193	.5893	5593
.2580	.5816	.5666	.3251	.5895	.5595
.2590	.5820	.5662	.3290	.5897	.5597
.2600	.5824	.5658	.3349	.5899	.5599
.2650	.5840	.5642	.3408	.5902	.5602
.2700	.5853	.5629	.3447	.5904	.5604
.2750	.5863	.5619	.3500	.5907	.5607

TABLE IV. - LEADING-EDGE COORDINATES - SPLITTER 2-4

Nondimensional distance from inlet highlight, X/R_h	Nondimensional distance from inlet axis		Nondimensional distance from inlet highlight, X/R_h	Nondimensional distance from inlet axis	
	For outside surface of splitter, R_o/R_h	For inside surface of splitter, R_i/R_h		For outside surface of splitter, R_o/R_h	For inside surface of splitter, R_i/R_h
0.5002	0.5900	0.5900	0.5300	0.6055	0.5794
.5005	.5913	.5385	.5350	.6065	.5792
.5010	.5923	5875	.5400	.6075	.5791
.5020	.5937	.5864	.5450	.6083	.5791
.5030	.5946	.5856	.5500	.6090	.5793
.5040	.5955	.5849	.5550	.6096	.5796
.5050	.5962	.5844	.5600	.6101	.5799
.5060	.5968	.5839	.5659	.6107	.5807
.5070	.5974	.5835	.5699	.6113	.5813
.5080	.5980	.5831	.5758	.6121	.5821
.5090	.5985	.5828	.5798	.6127	.5827
.5100	.5990	.5825	.5857	.6135	.5835
.5150	.6011	.5812	.5896	.6141	.5841
.5200	.6028	.5804	.5956	.6150	.5850
.5250	.6042	.5798	.6000	.6156	.5856

TABLE V. - LEADING-EDGE COORDINATES - SPLITTER 3-4

Nondimensional distance from inlet highlight, X/R_h	Nondimensional distance from inlet axis		Nondimensional distance from inlet highlight, X/R_h	Nondimensional distance from inlet axis	
	For outside surface of splitter, R_o/R_h	For inside surface of splitter, R_i/R_h		For outside surface of splitter, R_o/R_h	For inside surface of splitter, R_i/R_h
0.7508	0.6259	0.6259	0.7650	0.6381	0.6183
.7509	.6265	.6253	.7700	.6402	.6178
.7510	.6270	.6248	.7750	.6421	.6176
.7520	.6290	.6231	.7800	.6438	.6176
.7530	.6303	.6222	.7850	.6453	.6177
.7540	.6313	.6215	.7900	.6466	.6180
.7550	.6321	.6209	.7950	.6479	.6184
.7560	.6329	.6205	.8000	.6490	.6190
.7570	.6336	.6201	.8050	.6499	.6196
.7580	.6343	.6198	.8100	.6508	.6204
.7590	.6349	.6195	.8500	.6577	.6277
.7600	.6355	.6192			

TABLE VI. - MIDSECTION COORDINATES - SPLITTERS 1-2 AND 1-4

Nondimensional distance from inlet highlight, X/R_h	Nondimensional distance from inlet axis		Nondimensional distance from inlet highlight, X/R_h	Nondimensional distance from inlet axis	
	For outside surface of splitter, R_o/R_h	For inside surface of splitter, R_i/R_h		For outside surface of splitter, R_o/R_h	For inside surface of splitter, R_i/R_h
0.3500	0.5907	0.5607	0.7500	0.6402	0.6102
.4000	.5934	.5634	.8000	.6490	.6190
.4500	.5972	.5672	.8500	.6577	.6277
.5000	.6020	.5720	.9000	.6663	.6363
.5500	.6087	.5787	.9500	.6746	.6446
.6000	.6156	.5856	1.0000	.6825	.6525
.6500	.6233	.5933	1.0500	.6899	.6599
.7000	.6316	.6016	1.1000	.6967	.6667

TABLE VII. - MIDSECTION COORDINATES -

SPLITTER 2-4

Nondimensional distance from inlet highlight, X/R_h	Nondimensional distance from inlet axis	
	For outside surface of splitter, R_o/R_h	For inside surface of splitter, R_i/R_h
0.6000	0.6156	0.5856
.6500	.6233	.5933
.7000	.6316	.6016
.7500	.6402	.6102
.8000	.6490	.6190
.8500	.6577	.6277
.9000	.6663	.6363
.9500	.6746	.6446
1.0000	.6825	.6525
1.0500	.6899	.6599
1.1000	.6967	.6667

TABLE VIII. - MIDSECTION COORDINATES -

SPLITTER 3-4

Nondimensional distance from inlet highlight, X/R_h	Nondimensional distance from inlet axis	
	For outside surface of splitter, R_o/R_h	For inside surface of splitter, R_i/R_h
0.8500	0.6577	0.6277
.9000	.6663	.6363
.9500	.6746	.6446
1.0000	.6825	.6525
1.0500	.6899	.6599
1.1000	.6967	.6667

TABLE IX. - END SECTION COORDINATES -

SPLITTERS 1-2, 1-4, 2-4, AND 3-4

[0.002 R/R_h at trailing edge; center at
X/R_h = 1.2973, R/R_h = 0.7020.]

Nondimensional distance of outside surface from -		Nondimensional distance of inside surface from -	
Inlet highlight, X_o/R_h	Inlet axis, R_o/R_h	Inlet highlight, X_i/R_h	Inlet axis, R_i/R_h
1.1000	0.6967	1.1000	0.6667
1.1488	.7028	1.1512	.6732
1.1587	.7037	1.1612	.6742
1.1687	.7045	1.1711	.6752
1.1787	.7052	1.1810	.6765
1.1887	.7057	1.1910	.6778
1.1987	.7061	1.2009	.6794
1.2087	.7064	1.2108	.6809
1.2187	.7066	1.2206	.6827
1.2288	.7067	1.2305	.6844
1.2388	.7067	1.2404	.6863
1.2489	.7064	1.2502	.6885
1.2590	.7062	1.2601	.6906
1.2690	.7057	1.2699	.6930
1.2791	.7053	1.2797	.6953
1.2892	.7046	1.2895	.6970
1.2973	.7040	1.2973	.7000
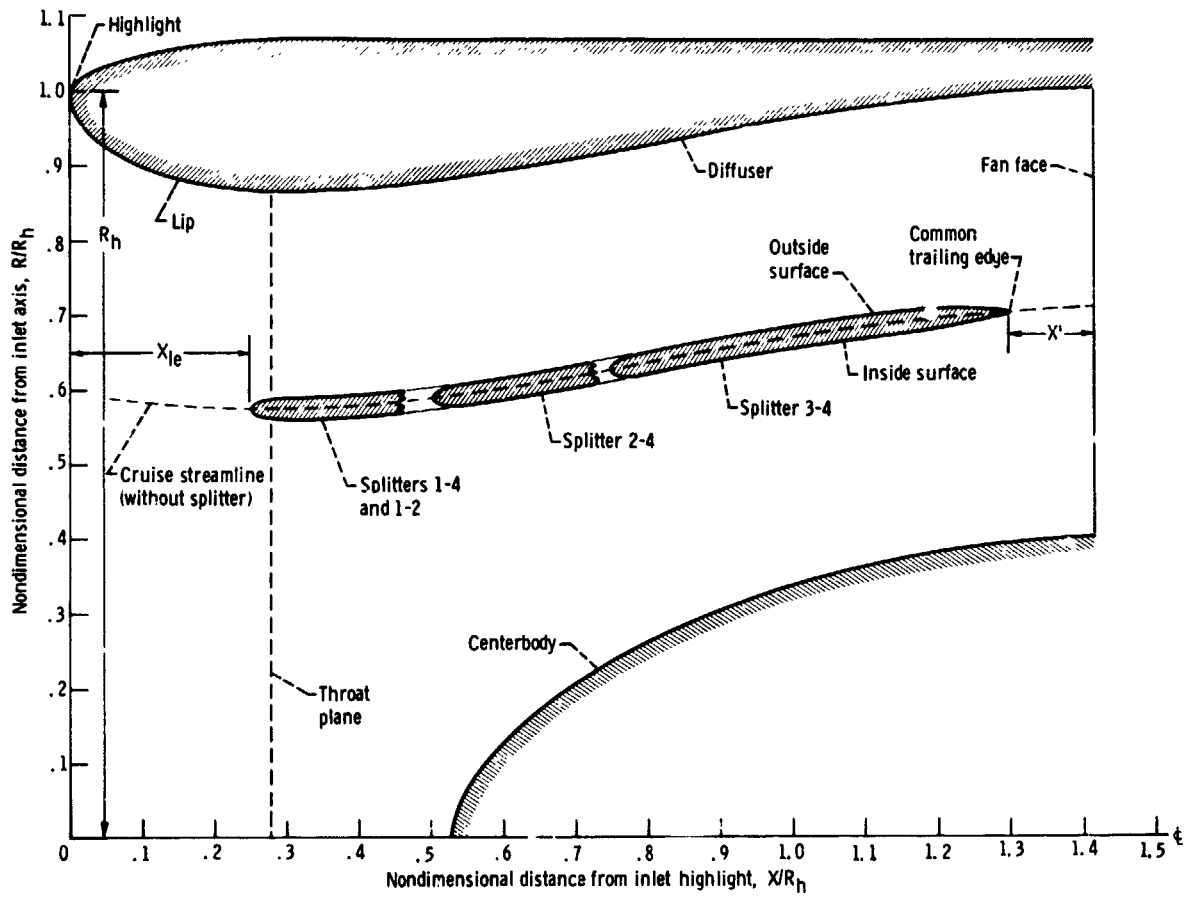
Figure 1. - Illustration of inlet with splitter geometries.
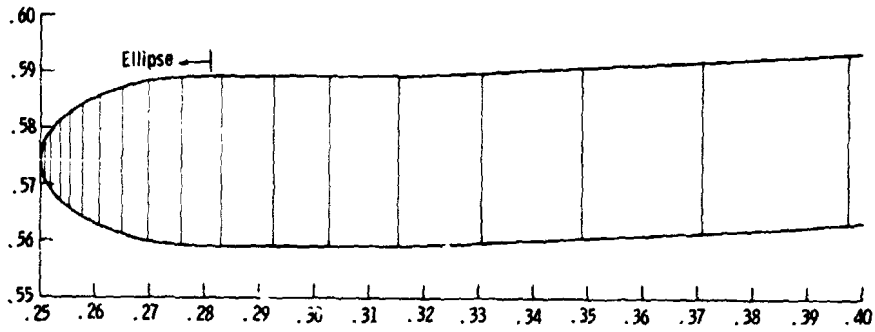
(a) Leading-edge splitter 1-2.

(b) Leading-edge splitter 1-4.

Nondimensional distance from inlet highlight, X/R_h
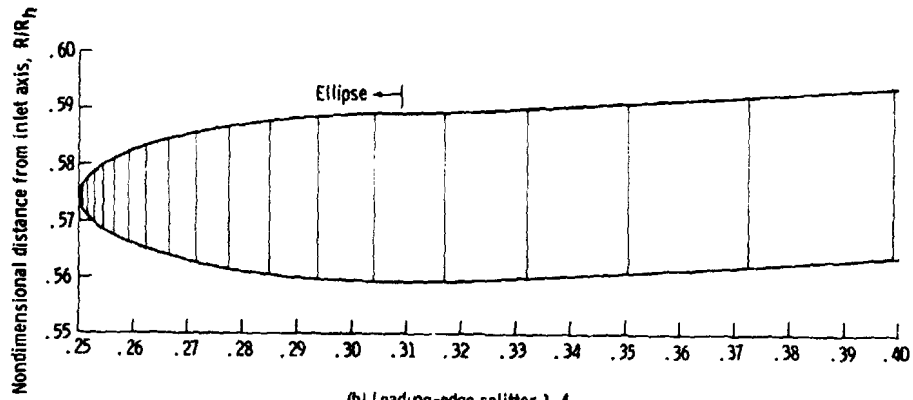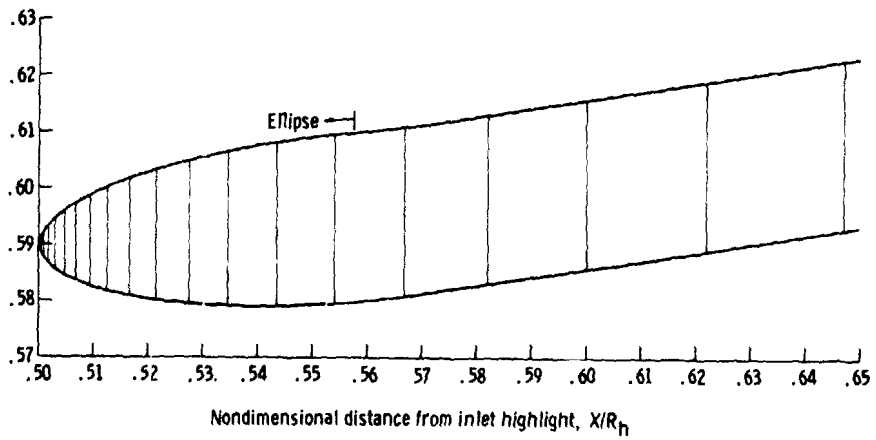
(c) Leading-edge splitter 2-4.

Figure 2. - Illustration of splitter leading and trailing edges.

(d) Leading-edge splitter 3-4.

Nondimensional distance from inlet highlight, X/R_h
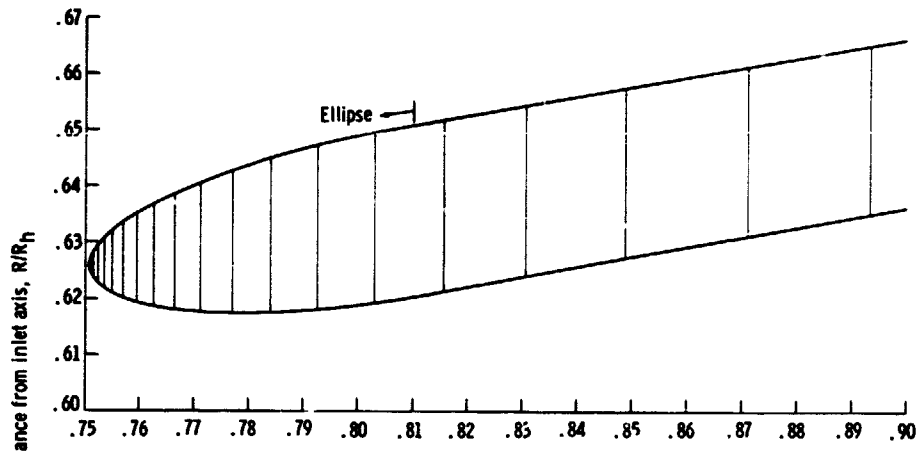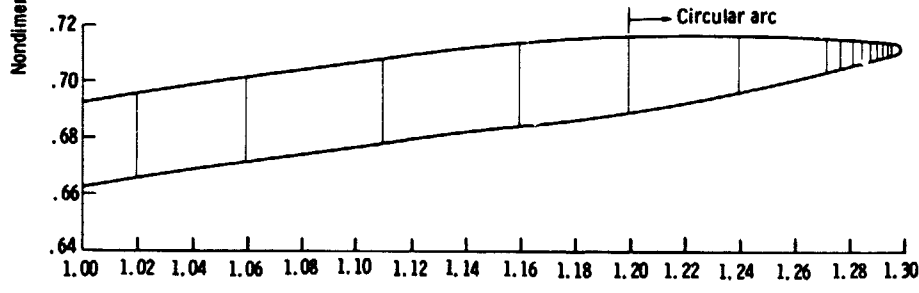
(e) Trailing-edge splitters 1-2, 1-4, 2-4, and 3-4.

Figure 2. - Concluded.
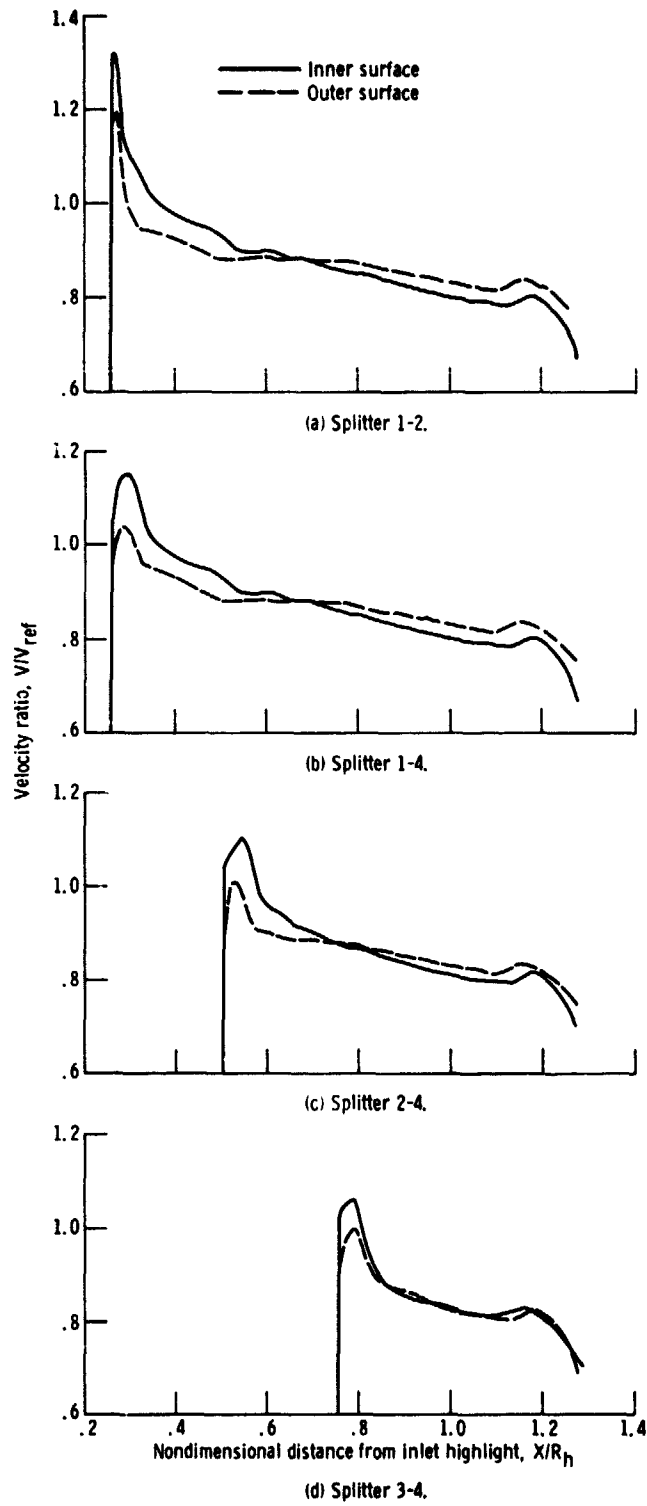
Figure 3. - Surface velocity distribution on inlet splitters at cruise condition. Inlet incidence angle, α, 0°; free-stream Mach number, 0.75; corrected weight flow per unit fan annular area, w_{cor}/A_f, 202 kg/(sec)(m²).

(a) Splitter 1-2.

(b) Splitter 1-4.

(c) Splitter 2-4.
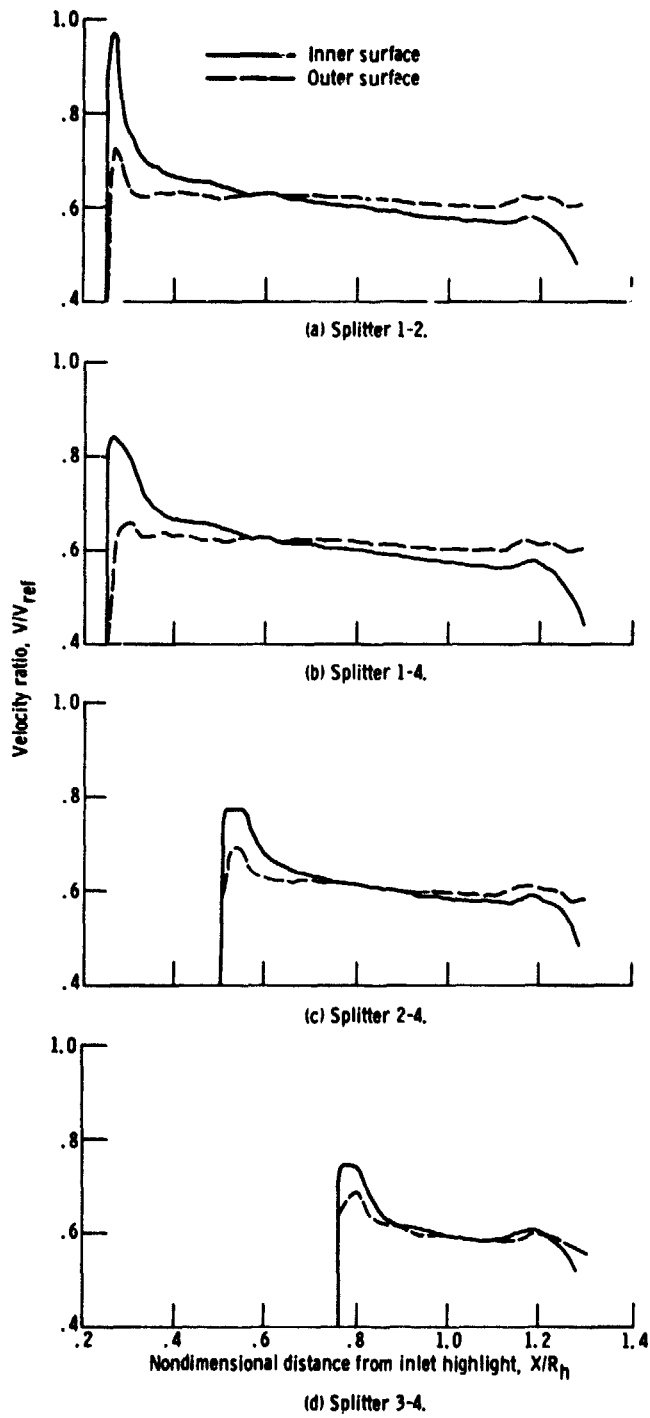
(d) Splitter 3-4.

Figure 4. - Surface velocity distribution on inlet splitters at low-speed
conditions with inlet incidence angle α of 0°. Free-stream Mach
number, 0.12; corrected weight flow per unit fan annular area,
w_{cor}/A_f, 175 kg/(sec×m²).

17
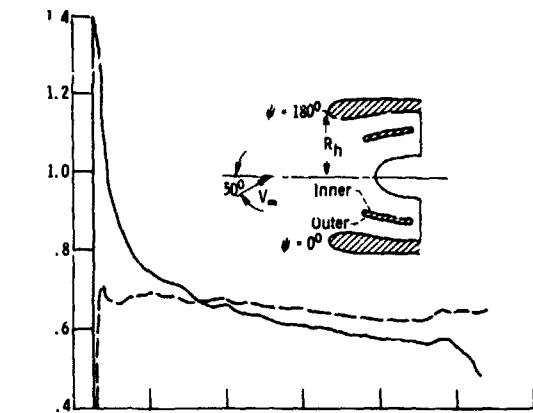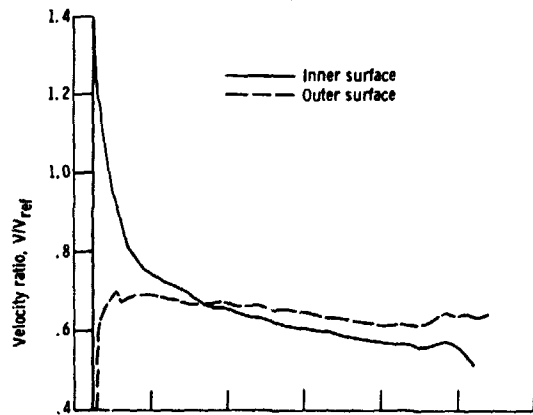
(a) Splitter 1-2.

(b) Splitter 1-4.
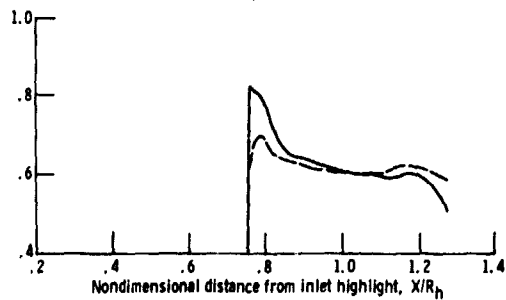
(c) Splitter 2-4.

(d) Splitter 3-4.

Figure 5. - Surface velocity distribution on inlet splitters at low-speed conditions with inlet incidence angle α of 50°. Free-stream Mach number, 0.12; corrected weight flow per unit fan annular area, w_{cor}/A_f, 175 kg/(sec)(m^2); circumferential angle, ψ, 0°.
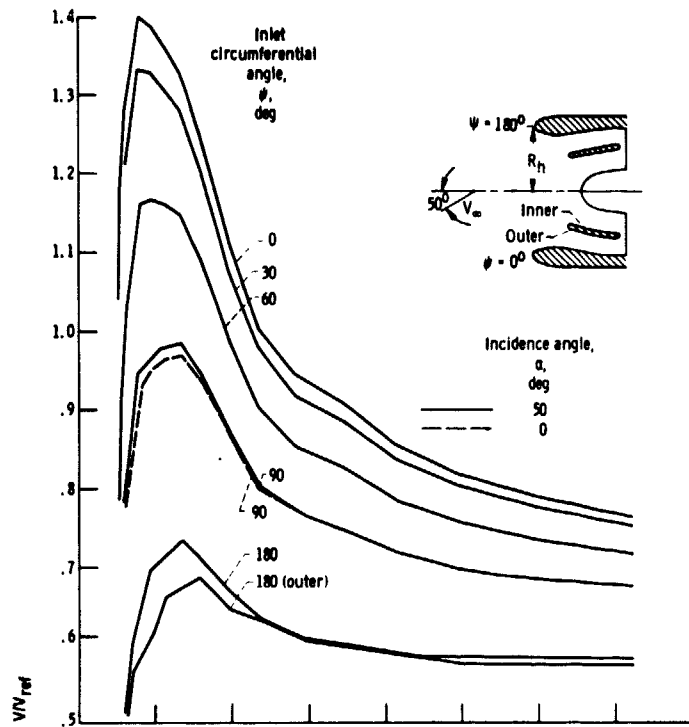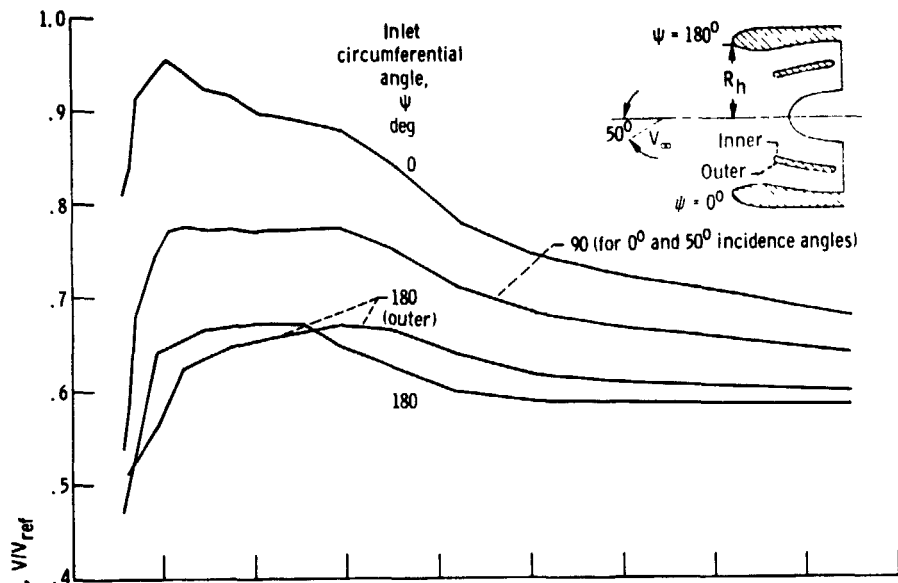
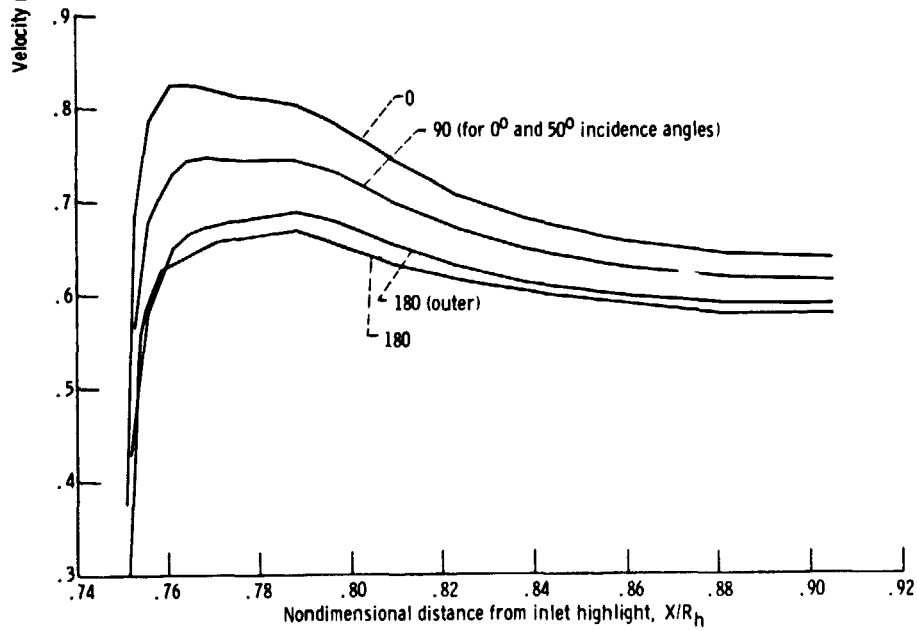(a) Splitter 1-2.
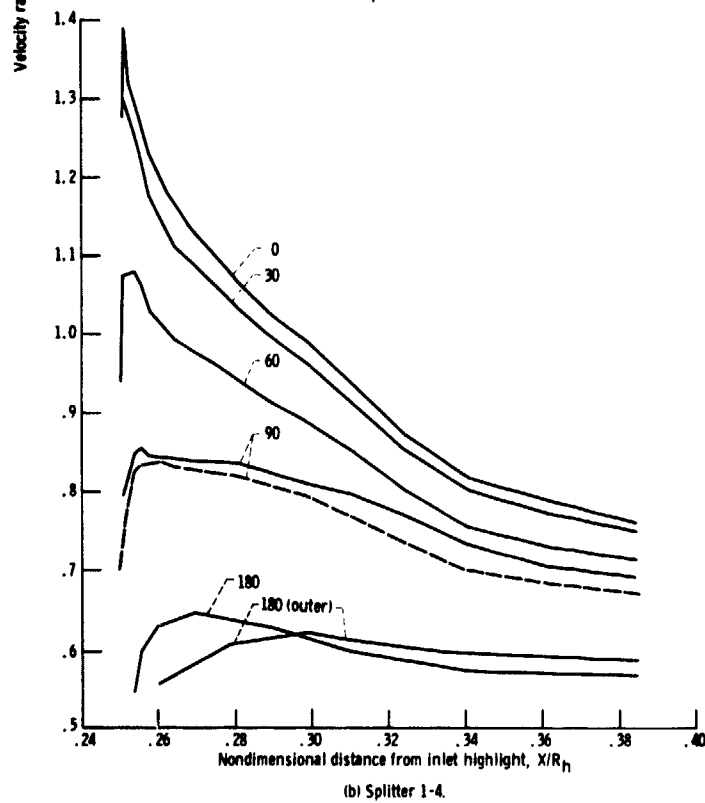
(b) Splitter 1-4.

Figure 6. - Surface velocity distribution on splitter inner surface for various circumferential angles. Free-stream Mach number, 0.12; corrected weight flow per unit fan annular area, w_{cor}/A_f, 175 kg/(sec×m²).

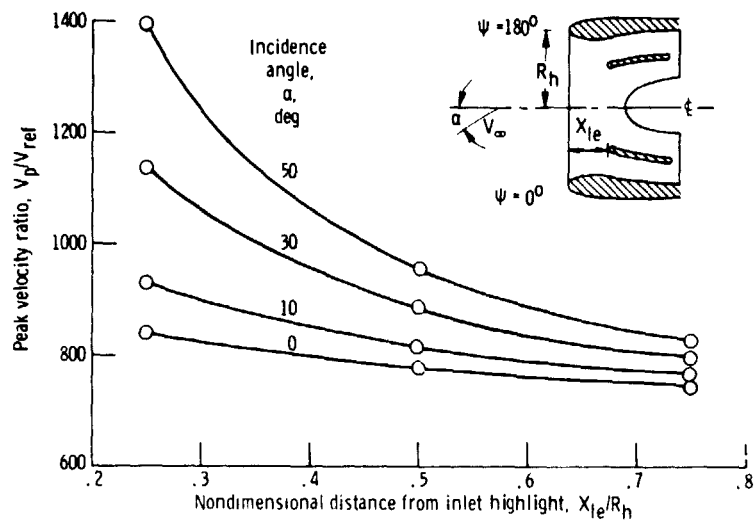(c) Splitter 2-4.

(d) Splitter 3-4.

Figure 6. – Concluded.

Figure 7. - Peak velocity variation on splitter inner surface at low-speed conditions. Splitter leading edge, 2-to-1 ellipse; free-stream Mach number, 0.12; inlet circumferential angle, ψ, 0°.